Electronic Supplementary Material (ESI) for Chemical Communications.


# Rotational dynamics of the imidazolium ion in cyanide-bridged dielectric framework materials

Anthony E. Phillips, Guanqun Cai and Franz Demmel

**Electronic Supplementary Information**

## Contents

# 1 Experimental details

The raw data from these experiments are freely available from the ISIS data repository at `https://doi.org/10.5286/ISIS.E.RB1620286` (Fe) and `https://doi.org/10.5286/ISIS.E.RB1720204` (Co).

The OSIRIS instrument is optimised for measurements of fast processes: using the PG002 reflection of the pyrolytic graphite analyser, the energy resolution function has a full width at half maximum of FWHM $= 25.4\,\mu$eV. This corresponds to a theoretical maximum timescale of around 140 ps for the processes observed. The PG004 reflection of the analyser gives a wider $Q$ range at the cost of lower energy resolution: here the resolution function has FWHM $= 99.0\,\mu$eV. Because this timescale excludes motion in the intermediate phases (Fig. 3(b)) and Bragg peaks contaminate much of the additional $Q$ range, this setting proved not to give useful data on these materials.

To confirm that the PG002 setting is adequate to distinguish between the possible structure models, we calculated the EISF for threefold, sixfold, and continuous circular rotation, as well as continuous spherical rotation for comparison (Fig. S1). (Note though that spherical rotation is inconsistent with the crystallographic structure.) As noted in the main text, the sixfold and continuous rotation models are indistinguishable with this $Q$ range; however, the threefold, sixfold or higher, and spherical models are clearly different. Indeed, the data clearly give a very poor fit to the spherical model, worse than any model described in the main text (Fig. S2).

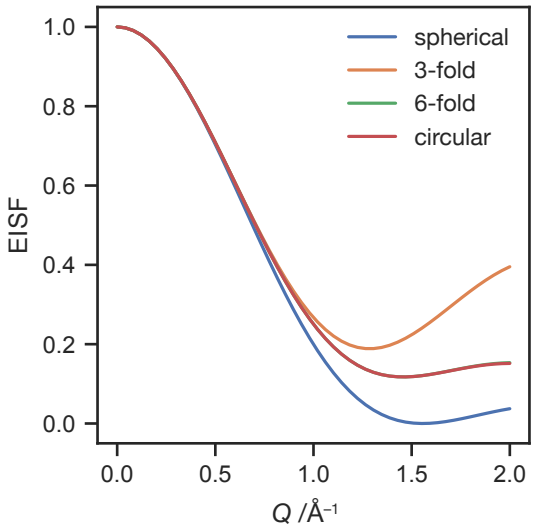


**Figure S1:** EISFs for four rotation models, calculated using the imidazolium ion radius $r = 2.018\,$Å. The PG002 analyser setting on OSIRIS, which allows measurement up to $Q_{\mathrm{max}} \approx 2\,\text{Å}^{-1}$, is adequate to distinguish between all of these models except sixfold and circular rotation.

Data were initially processed in Mantid. We used the MSDFit algorithm to calculate $\langle u^2 \rangle$, first integrating the elastic window scan over the energy transfer range $-25\,\mu\text{eV} \leq \omega \leq 25\,\mu\text{eV}$, then extracting $\langle u^2 \rangle$ through a linear fit of the logarithm of the intensity against $Q^2$ (see eq. 1) in the range $0.24\,\text{Å}^{-1} \leq Q \leq 1.27\,\text{Å}^{-1}$ at each temperature. We used a Bayesian fit algorithm, "Quasi", to fit $S(Q,\omega)$ (eq. 1) to the measured spectra. The model was numerically convolved with a measured resolution function to take into account

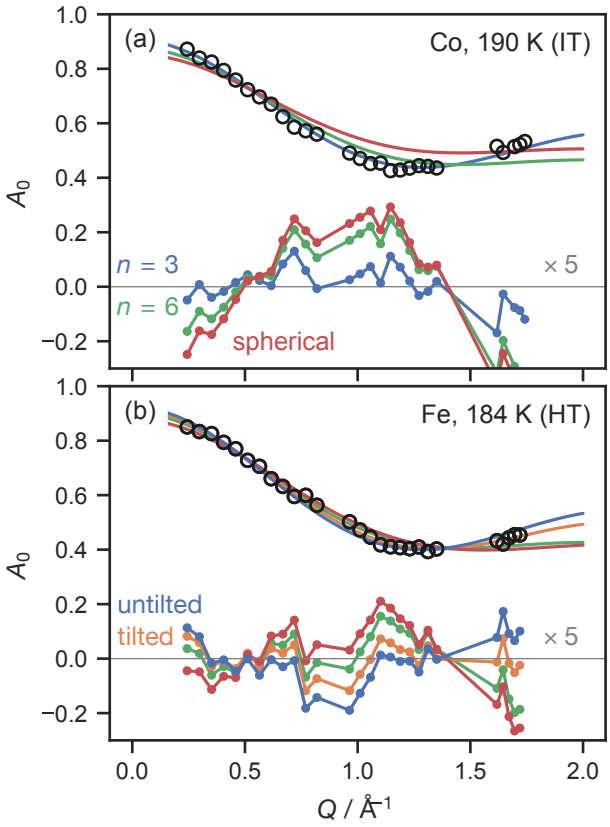


**Figure S2:** The data of Fig. 1(c) and (d), replotted together with fits to an isotropic spherical rotation model $A_0 = j_0(Qr)^2$. The spherical model gives a worse fit than any model discussed in the main text.

the broadening from the spectrometer. The resolution function was obtained from a low temperature measurement ($T = 10\,\mathrm{K}$), where no motion occurs on the time scale of the spectrometer. The scattering factors $A_l(Q)$ and correlation times $\tau_l$ were determined from the fit.

Representative fits are shown in Fig. S3. Although the two-Lorentzian fit gives a smaller and less structured residual when considering this single detector (*i.e.*, $Q$ value) alone, it is not clear that this is physically meaningful. As discussed below, neither the inelastic structure factor $A_2(Q)$ nor the time constant $\tau_2$ obtained from this analysis were reasonable. We therefore used a single-Lorentzian model for all of the analysis reported here.

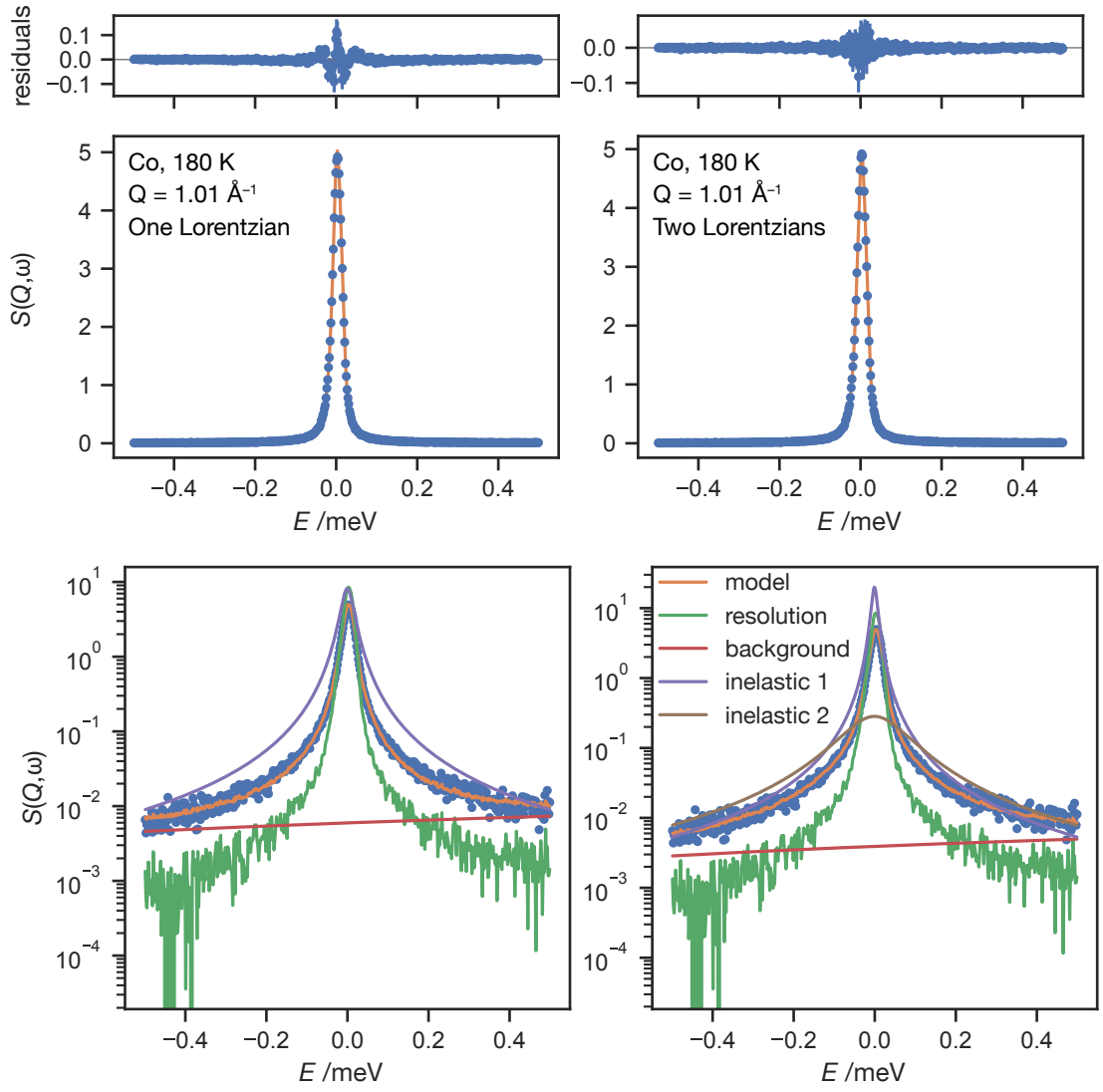


**Figure S3:** Representative fits to a one- (left) and two-Lorentzian (right) model. Top: overall fits on a linear intensity scale. Bottom: the same fits, decomposed into components and on a logarithmic intensity scale.

Subsequent fitting was performed in Python, using the `lmfit` and `qef` modules.

## 2 Simple EISF for the tilted geometry

We take the axis about which the ion rotates to be the $z$ axis and the axis about which it tilts to be the $x$ axis. We begin by arranging the imidazolium ion, which we approximate as a regular pentagon, in a circle of radius $r$ in the $xy$ plane:

$$\mathbf{r}_i = \big(r\cos(\phi_i+\xi), r\sin(\phi_i+\xi), 0\big) \tag{1}$$

$$\phi_i = \frac{2\pi}{5}i \qquad i = 1,\ldots,5 \tag{2}$$

Here $\xi$ represents the orientation of the imidazolium ion with respect to the tilting axis; we include this parameter for the sake of generality, although we will show that its value does not affect the derived EISF.

We now rotate by an angle $\theta$ about the $x$ axis:

$$\mathbf{r}_i = \big(r\cos(\phi_i+\xi), r\sin(\phi_i+\xi)\cos\theta, r\sin(\phi_i+\xi)\sin\theta\big) \tag{3}$$

The radius of rotation is then given by

$$r_i^{\mathrm{rot}} = \sqrt{x_i^2+y_i^2} \tag{4}$$

$$= r\sqrt{\cos^2(\phi_i+\xi)+\sin^2(\phi_i+\xi)\cos^2\theta}. \tag{5}$$

We now substitute this into the standard expression for the EISF for hopping around a circle, taking the average of the EISFs due to each of the five protons. For concreteness we use a three-site model here, although the same calculation can be done for any number of sites:

$$A_0(Q) = \tfrac{1}{5}\sum_{i=1}^{5}\tfrac{1}{3}\big[1+2j_0\big(\sqrt{3}Qr_i(\theta)\big)\big]. \tag{6}$$

The dependence of the resulting EISF on $\theta$ is plotted in Fig. S4. It is a rather complex mathematical expression if expanded in full, so rather than attempting to prove independence from $\xi$ analytically, we demonstrate this numerically in Fig. S5.

If we incorporate hopping between tilt angles $\pm\theta$, the EISF becomes

$$A_0(Q) = \tfrac{1}{6}\big(1+2j_0(Qr_3)+j_0(Qr_2)+2j_0(Qr_d)\big) \tag{7}$$

where $r_3$ is the distance between sites around the threefold axis, $r_2$ between sites with opposite tilt angles, and $r_d$ the "diagonal" between them:

$$r_3 = \sqrt{3}r\sqrt{\cos^2\phi+\sin^2\phi\cos^2\theta} \tag{8}$$

$$r_2 = 2r\sin\phi\sin\theta \tag{9}$$

$$r_d = \sqrt{r_3^2+r_2^2} \tag{10}$$

This barely changes the EISF from the simpler version given in the main text, and the refined parameters do not change within experimental error.

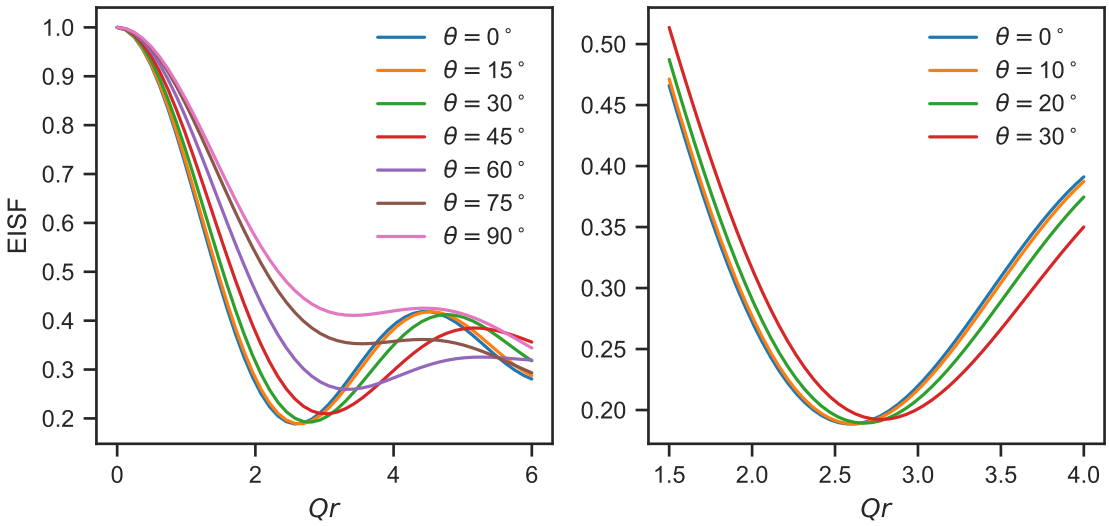


**Figure S4:** Variation of the tilted three-site EISF with $\theta$.

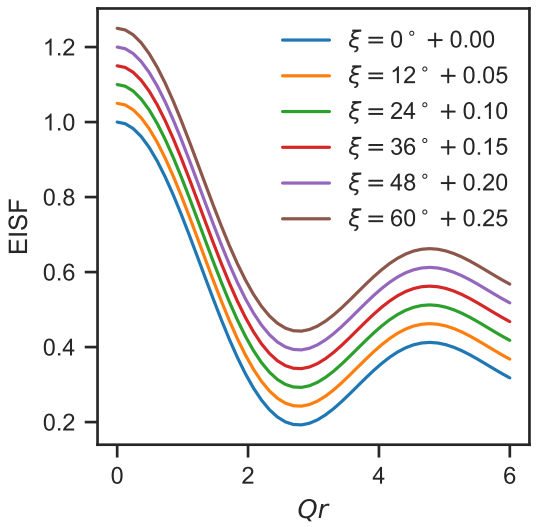


**Figure S5:** (No) variation of the tilted three-site EISF with $\xi$. A small offset has been applied as indicated to differentiate the curves from one another. Here $\theta = 30°$.

This model implies that there should be *two* inelastic structure factors, with corresponding time constants

$$\tau_E^{-1} = \frac{3}{\tau_3} + \frac{3}{\tau_2} \tag{11}$$

$$\tau_{A_2}^{-1} = \frac{6}{\tau_2} \tag{12}$$

where $\tau_2$ and $\tau_3$ are the correlation times for hopping about the twofold and threefold axes respectively. Although, as noted above, in some cases a two-Lorentzian model appeared to give a better fit for individual detectors, we were unable consistently to extract two reasonable inelastic structure factors from the data. Moreover, where we did, the greater FWHM (corresponding to faster motion) was at least around 5 times as large as the smaller, whereas it is clear from equations 11 and 12 that the greatest possible ratio between the two correlation times in this model is 2. As a result, we performed our final analysis based on a single-Lorentzian fit, assuming that hopping between tilt angles $\pm\theta$ is negligibly fast.

## 3 Simple EISF fitting

As noted in the caption to Fig. 2 in the main text, the uncertainty in the tilt angle $\theta$ is poorly estimated from the covariance matrix when this angle refines to zero. To establish realistic confidence limits for the fit, we therefore performed Markov chain Monte Carlo modelling using the `pymc3` Python package. The prior distributions were taken as follows:

$$\begin{aligned}
\tan\theta &\sim \text{Exponential}(\lambda = 2.75) \\
f &\sim \text{Uniform}(0, 1) \\
m &\sim \text{Beta}(\mu = 0.9, \sigma = 0.1) \\
\text{error scale} &\sim \text{Lognormal}(\mu = 2.78, \sigma = 1.0) \\
\text{EISF} &\sim \text{Normal}(\mu = \text{observed values}, \sigma = \text{esds from Mantid} \times \text{error scale})
\end{aligned}$$

The "error scale" parameter was introduced to compensate for underestimation of the true uncertainties in the Mantid processing steps; it refined to approximately 4.

The results are shown for two representative data sets in Fig. S6, clearly demonstrating a qualitative difference between the two phases.

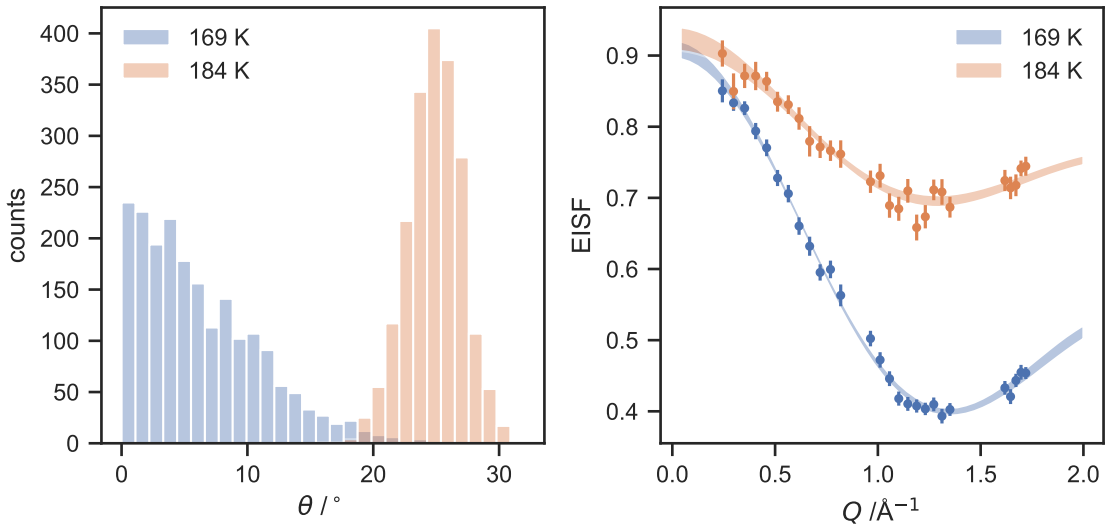


**Figure S6:** Left: Posterior distribution of the $\theta$ angle for two representative fits, in the IT and HT phase of the Fe material. Right: Corresponding 95% confidence interval for the "true" EISF.